

Fourier Transform Spectroscopy of the O₂ Herzberg Bands. III. Absorption Cross Sections of the Collision-Induced Bands and of the Herzberg Continuum

S. Fally,* A. C. Vandaele,^{†,1} M. Carleer,* C. Hermans,[†] A. Jenouvrier,[‡] M.-F. Mérienne,[‡]
B. Coquart,[‡] and R. Colin*

*Université Libre de Bruxelles, Laboratoire de Chimie Physique Moléculaire, CP160/09, 50 Av. F. D. Roosevelt, B-1050 Brussels, Belgium; [†]Institut d'Aéronomie Spatiale de Belgique, 3 Av. Circulaire, B-1180 Brussels, Belgium; and [‡]Université de Reims Champagne-Ardenne, Groupe de Spectrométrie Moléculaire et Atmosphérique, UPRESA 6089, UFR Sciences, Moulin de la Housse, B.P. 1039, F-51687 Reims Cedex 2, France

Received March 8, 2000; in revised form July 11, 2000

Absorption spectra of molecular oxygen were measured in the laboratory under temperature and pressure conditions prevailing in the Earth's atmosphere. Spectra of pure O₂, O₂ + N₂, and O₂ + Ar were recorded in the 41 700 to 33 000 cm⁻¹ region (240–300 nm) at a maximal optical path difference of 0.45 cm using a Fourier transform spectrometer and a multiple reflection gas cell. The different components of the spectra, namely the discrete bands of the three Herzberg systems, the Herzberg continuum, and the collision-induced diffuse Wulf bands, were separated. The contribution of the Herzberg bands was first subtracted using the line parameters determined previously [A. Jenouvrier, M.-F. Mérienne, B. Coquart, M. Carleer, S. Fally, A. C. Vandaele, C. Hermans, and R. Colin, *J. Mol. Spectrosc.* **198**, 136–162 (1999)] from high-resolution data. Spectra recorded at various pressures then made it possible to determine by linear regression the intensity of the Wulf bands and the Herzberg continuum. The characteristics of the Wulf bands have been investigated in details: vibrational analysis, pressure effect, foreign gas effect, and a simulated spectrum are reported. The Herzberg continuum cross section is determined below the dissociation limit. A comparison with literature data is given. The new O₂ absorption cross sections and O₂–O₂ collision-induced absorption cross sections are useful in connection with atmospheric measurements of ozone and other trace gases in the UV spectral region. © 2000 Academic Press

Key Words: oxygen; absorption cross section; collision-induced bands; Fourier transform spectroscopy; UV; Herzberg continuum; Wulf bands.

1. INTRODUCTION

Accurate retrieval of atmospheric trace gas concentrations and vertical profiles from UV–visible spectra require the knowledge of absolute absorption cross sections of all absorbing species, including oxygen. Laboratory-measured cross sections are thus essential as reference data for tropospheric and stratospheric monitoring from the ground, balloons and aircraft platforms, and satellites. Furthermore, the radiative budget of the atmosphere, which influences the global climate, is controlled by the absorption of solar radiation by trace gases.

The strong ozone Hartley band (230–300 nm), which is used to retrieve tropospheric ozone concentrations (1, 2), overlaps with oxygen bands. Despite the low-absorption cross section of oxygen in this region ($\sim 10^{-24}$ cm² molecule⁻¹ compared to $\sim 10^{-17}$ cm² molecule⁻¹ for ozone), the abundance of oxygen in the atmosphere leads to absorbances of the same order of magnitude as those of O₃. Reliable ozone concentration measurements thus require the knowledge of accurate oxygen cross

sections. Similarly, concentration measurements of aromatic species by DOAS or DIAL techniques require the elimination of oxygen absorptions from atmospheric spectra (3).

The absorption spectrum of molecular oxygen between 33 000 and 41 700 cm⁻¹ is composed of the discrete Herzberg I, II, III band systems ($A^3\Sigma_u^+ - X^3\Sigma_g^-$, $c^1\Sigma_u^- - X^3\Sigma_g^-$, and $A'^3\Delta_u - X^3\Sigma_g^-$ transitions), the weak underlying Herzberg continuum, and the broad collision-induced absorption bands with triplet structure (4–7) attributed to O₂–O₂ and O₂–X. The latter were observed in the 1920s–1930s at high pressures in the gas phase and in liquid oxygen (8–10). Wulf (8) first ascribed these so-called high-pressure bands to the formation of oxygen dimers. Later, several authors studied the pressure dependence of their cross sections in pure oxygen as well as in the presence of a foreign gas, e.g., N₂, Ar, CO₂ (11–19). They demonstrated the quadratic pressure dependence of the Wulf band intensities and discussed the nature of the O₂–X interaction. The triplet bands were attributed either to a stable dimer or to a colliding pair. Various studies (6, 20–22) suggested that the triplet structure of the Wulf bands originates from the collision-induced relaxation of the selection rules for the $A'^3\Delta_u \leftarrow X^3\Sigma_g^-$ electric dipole forbidden transition. Our recent experimental work (23) led us to conclude that the Wulf bands are

¹ Postdoctoral Researcher with the Fonds National de la Recherche Scientifique (Belgium).

caused by collision-induced absorption (CIA) rather than by oxygen dimers. This will be confirmed in the present paper.

Concerning the continuous absorptions, we would like to specify the terminology used in this work. Up to now, the Herzberg continuum, generally measured from 195–200 nm to the dissociation limit (240 nm), was considered to be the sum of a pressure-independent and a pressure-dependent contribution. These two contributions have no specific name. We suggest to label the pressure-independent term the *Herzberg continuum* and to be aware that it has a contribution in the bound region below the dissociation limit. The pressure-dependent contribution below the dissociation limit will be designated as the *Wulf bands* and above the dissociation limit as the *Wulf continuum*. The sum of the pressure-dependent and -independent terms (called earlier the Herzberg continuum) will simply be called the *dissociation continuum*.

This study, which is part of a complete reinvestigation of the entire O₂ spectrum from the UV to the near-IR (23–26), is based on low-resolution spectra recorded at atmospheric pressures in the UV region (33 000–42 000 cm⁻¹). The objective is to subtract the contribution of the discrete Herzberg bands and to determine the intensity of the collision-induced absorption bands up to the dissociation limit. This will make use of the previous high-resolution rotational analysis of the Herzberg bands carried out by us (24, 25). Cross sections for the O₂–O₂ bands will be provided and the effect of foreign gases (N₂, Ar) will be presented and interpreted. Removal of the lines of the Herzberg bands enables us to measure the Wulf bands at atmospheric pressures, as opposed to previous studies, which were carried out at higher pressures at which the Herzberg bands were assumed to be negligible.

2. EXPERIMENTAL

The absorption spectra of gaseous molecular oxygen were recorded using a Bruker IFS120M Fourier transform spectrometer (FTS) combined with a multiple reflection cell of 50-m base path. The cell characteristics and configuration were described in detail by Lux and Jenouvrier (27).

The experimental conditions, which are summarized in Table 1, are the result of a compromise between a reasonable measuring time (~1 h) and a good signal-to-noise ratio. It was decided to operate at low resolution ($R = 2 \text{ cm}^{-1}$; MOPD = 0.45 cm) because the present study concerns continuous absorptions. The overlapping discrete Herzberg bands will be removed from the low-resolution spectra by using the high-resolution (fully resolved) spectra which were recorded previously (24).

In practice, spectral intensities (I) were recorded for a series of pressures, and a blank spectrum (empty cell) was measured before and after each series (I_0). Each spectrum was recorded in eight blocks of 128 scans in order to be able to eventually discard erroneous blocks, and to monitor the lamp drift with time. The problem of lamp aging was examined in an attempt to predict the values of I_0 at the exact time of a particular

TABLE 1
Experimental Conditions for the
Absorption Measurements

Cell base length (m)	50
Absorption path length (m)	201.9, 402.1, 602.3
Spectral region (cm ⁻¹)	33000–42000
Lamp	Xe (Not O ₃ free, 450 W, 950 W, Ushio)
Detector	solar blind UV vacuum diode
Temperature (K)	287.0 - 289.7
Pressure range (hPa)	100 to 1000 (pure) 400 to 1013 (20% O ₂ , 80% N ₂ or Ar)
Resolution (cm ⁻¹)	2
Maximal optical path difference (cm)	0.45
Number of co-added scans	1024
Recording time per experiment (min)	60

sample block measurement. It was found that I_0 varies by 0.3–2.0% over the recording time of eight blocks, but does not vary linearly with time, preventing linear interpolation. The average of the 16 blocks of blanks was therefore used.

Measurements were carried out at room temperature and at pressures less than, or equal to, 1 atm. Three platinum wire resistance thermometers placed inside the cell measured the gas temperature. The temperature difference between the three thermometers never exceeded 2 K; the temperature variation during one experiment (sample and blank spectra) was negligible. The pressure was monitored by an MKS Baratron capacitance manometer with a calibrated full-scale sensor of 133 or 1333 hPa.

The samples studied were either pure O₂, dry synthetic air from commercial bottles (O₂ = 20 ± 1%), O₂/N₂ mixtures, or O₂/Ar mixtures. The two mixtures were prepared directly in the cell by successively introducing the oxygen and the buffer gas (the pure O₂, N₂, and Ar having a certified purity >99.5%). The results obtained with dry synthetic air and O₂/N₂ mixtures prepared directly in the cell and left to rest for 2 h were the same. Two hours appears therefore to be sufficient to achieve a homogeneous mixture.

Spectra were recorded by using the double-sided forward–backward recording mode of the FTS and a boxcar apodization function.

3. RESULTS AND DISCUSSION

3.1. Separation between Structured and Diffuse Bands

The absorbance A , calculated from the measured intensities I and I_0 , is related to the oxygen pressure as

$$A = \ln\left(\frac{I_0}{I}\right) = (\sigma_{\text{O}_2\text{HS}} + \sigma_{\text{O}_2\text{HC}}) P_{\text{O}_2} l k + (\sigma_{\text{O}_2-\text{O}_2} + \sigma_{\text{O}_2-X} \gamma) P_{\text{O}_2}^2 l k^2 + A_{\text{RS}}, \quad [1]$$

where A is the Napierian absorbance, I is the sample spectrum intensity, I_0 is the blank spectrum intensity, $\sigma_{\text{O}_2\text{HS}}$ and $\sigma_{\text{O}_2\text{HC}}$ are the Herzberg band systems and Herzberg continuum absorp-

tion cross sections, respectively ($\text{cm}^2 \text{ molecule}^{-1}$), $\sigma_{\text{O}_2\text{-O}_2}$ and $\sigma_{\text{O}_2\text{-X}}$ are the collision-induced absorption cross sections ($\text{cm}^5 \text{ molecule}^{-2}$), l is the path length (cm), P_{O_2} is the oxygen pressure (hPa), γ is the X/O_2 mixing ratio, A_{RS} is the absorbance equivalent to the photon loss due to Rayleigh scattering, and k is equal to $N_0 T_0 / P_0 T$ where N_0 is the Loschmidt number ($2.687 \times 10^{19} \text{ molecule cm}^{-3}$), T_0 and P_0 are the normal temperature and pressure (K and hPa), and T is the sample temperature (K). For pure O_2 experiments, γ equals zero. The total pressure of the $\text{O}_2\text{-X}$ mixture experiments was varied, but the value of γ was maintained constant and close to the atmospheric N_2/O_2 ratio (≈ 4).

On the right-hand side of Eq. [1], the first term varies linearly with pressure and is composed of the absorption cross sections of the three Herzberg systems $\sigma_{\text{O}_2\text{HS}}$ and of the Herzberg continuum $\sigma_{\text{O}_2\text{HC}}$. The second term corresponds to the quadratic pressure-dependent part of the absorbance and is due to $\text{O}_2\text{-O}_2$ and $\text{O}_2\text{-X}$ ($X = \text{N}_2$ or Ar) collision-induced absorptions.

It follows from Eq. [1] that the effective oxygen cross section, which includes the three contributions to the spectrum (i.e., the Wulf bands, the discrete Herzberg bands, and the Herzberg continuum), is given by:

$$\sigma_{\text{eff}} = \frac{A - A_{\text{RS}}}{P_{\text{O}_2} l k} \quad [2]$$

Measurements at various pressures from 100 to 1000 hPa allowed us to separate the three components of the spectrum by the following procedure:

(a) Absorbance equivalent to the photon loss due to the Rayleigh scattering is calculated according to the equations given by Bates (28) and subtracted from the experimental absorbance (Fig. 1a).

(b) A low-resolution (2 cm^{-1}) absorbance spectrum of the O_2 Herzberg lines is calculated (Fig. 1b) with the Winprof program written by Hurtmans (29). This computer program synthesizes a spectrum by applying a Voigt line profile to theoretical values of the line positions and intensities. It then convolves this spectrum with the instrumental effects (truncation, apodization, and field of view) in order to match as closely as possible the experimental data. In the present work, the line parameters were determined from our high-resolution study (24, 25) and can be obtained upon request or by download from the IASB-BIRA website (<http://www.oma.be/BIRA-IASB/Scientific/Topics/Lower/LaboBase/Laboratory.html>).

(c) To remove the Herzberg lines, the difference between the experimental absorbance and the calculated absorbance is calculated and smoothed using a low-pass filter. This filtered difference is expressed in cross-section units and can be written as:

$$\sigma' = \sigma_{\text{O}_2\text{HC}} + (\sigma_{\text{O}_2\text{-O}_2} + \sigma_{\text{O}_2\text{-X}} \gamma) P_{\text{O}_2} k. \quad [3]$$

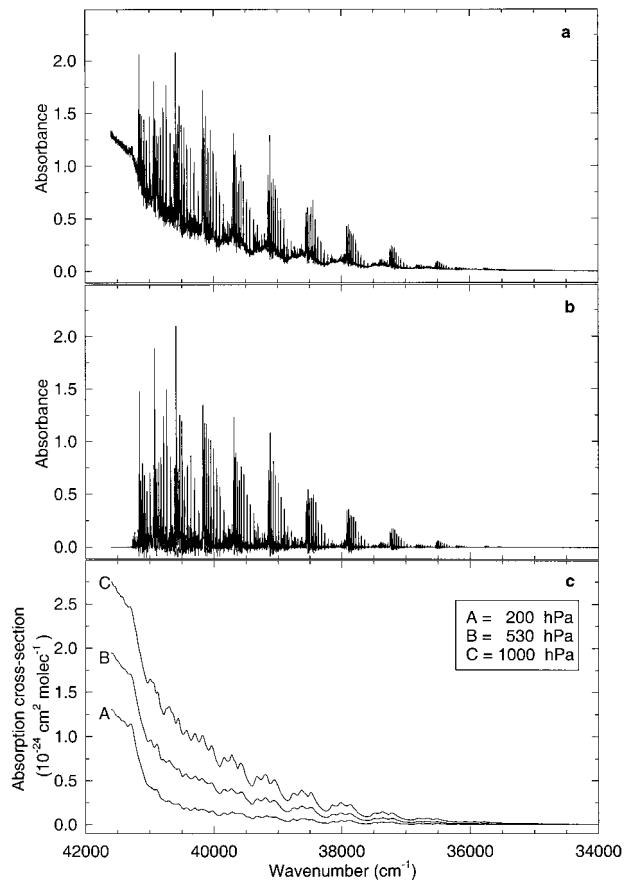


FIG. 1. (a) Overview of an experimental absorbance spectrum of pure oxygen at 600 hPa (resolution = 2 cm^{-1}). (b) Simulated absorbance spectrum at the same pressure and resolution. (c) Examples of σ' (see text) at three different O_2 pressures.

Steps (a) to (c) are repeated for spectra recorded at several pressures (Fig. 1c). For pure O_2 experiments, a set of 50 σ' values (corresponding to 17 pressures) was obtained during three different measurement periods. Preliminary results from the first period have been presented previously (23, 30, 31). Erroneous data, due to experimental and technical problems, such as clipping of the light beam emerging from the cell, were discarded, and the final data set is restricted to 21 values corresponding to 14 pressures.

(d) For experiments with pure O_2 , a linear least-squares fit of σ' versus P_{O_2} is performed for each measured wavenumber. The slope, divided by k , yields the collision-induced cross-section $\sigma_{\text{O}_2\text{-O}_2}$ (Fig. 2a) and the intercept at zero pressure provides the Herzberg continuum cross-section $\sigma_{\text{O}_2\text{HC}}$ (Fig. 2b).

(e) For the experiments with $\text{O}_2\text{-X}$ mixtures, the limited data set prevents the performance of a least-squares fit. Therefore, a value of the collision-induced absorption cross-section $\sigma_{\text{O}_2\text{-X}}$ is obtained by using Eq. [3], in which $\sigma_{\text{O}_2\text{-O}_2}$ and $\sigma_{\text{O}_2\text{HC}}$ are determined using procedure (d).

It should be emphasized that the proper removal of the

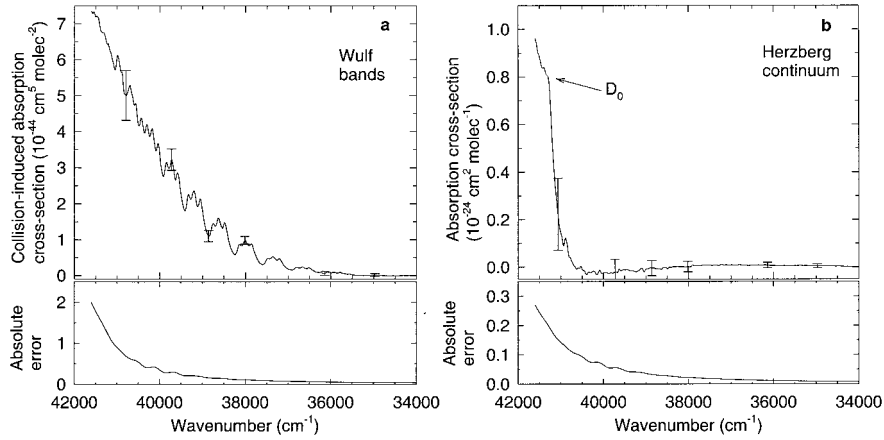


FIG. 2. (a) The O₂–O₂ collision-induced absorption cross-section $\sigma_{O_2-O_2}$. (b) The Herzberg continuum absorption cross-section σ_{O_2HC} . Standard deviations of the cross sections are shown and plotted as error bars for a few points on the main graphs. Also shown on plot (b) is the dissociation limit D_0 .

Herzberg lines is an essential prerequisite to study accurately the Wulf bands. The reason lies in saturation and resolution effects. First, the strongest Herzberg lines are saturated even at low-oxygen pressure, but saturated lines are only detectable at high resolution. Second, the Herzberg lines are not fully resolved in the low-resolution spectra (2 cm^{-1}). This implies that the line profile does not vary linearly with oxygen pressure (3). These specific problems result in strong line residuals in the linear least-squares fit, as was already demonstrated (31). A line-by-line removal of the Herzberg bands and a smoothing of the result give a much better result, but the O₂–O₂ collision-induced absorption cross section still presents some residual noise (see Fig. 3 in Ref. 23).

3.2. Error Analysis

The error in the effective cross-section σ_{eff} is determined using the expressions

$$\frac{\delta\sigma_{\text{eff}}}{\sigma_{\text{eff}}} = \frac{\delta A}{A} + \frac{\delta T}{T} + \frac{\delta P_{\text{tot}}}{P_{\text{tot}}} + \frac{\delta l}{l} \quad [4]$$

with

$$\delta A = N \left(\frac{1}{I} + \frac{1}{I_0} \right),$$

where N is the noise of a spectrum resulting from 1024 coadded scans. In Eq. [4], $\delta T/T$, $\delta P_{\text{tot}}/P_{\text{tot}}$, and $\delta l/l$ are equal to 1, 0.08, and 0.5%, respectively. The error in the modified cross section ($\delta\sigma'$) is obtained by filtering $\delta\sigma_{\text{eff}}$ with the same low-pass filter as the one used for the data. Errors in the slope and intercept obtained from the least-squares fitting are determined with the formula recommended by Press *et al.* (32) which is applicable when the uncertainty associated with each measurement is known. The error in the collision-induced

absorption cross-section $\delta\sigma_{O_2-O_2}$ (Fig. 2a, lower graph and error bars) is obtained from the standard deviation on the slope (δs) as

$$\frac{\delta\sigma_{O_2-O_2}}{\sigma_{O_2-O_2}} = \frac{\delta s}{s} + \frac{\delta T}{T}, \quad [5]$$

where $\delta T/T$ is negligible with respect to $\delta s/s$.

The error in the Herzberg continuum absorption cross-section $\delta\sigma_{O_2HC}$ is equal to the standard deviation on the intercept (Fig. 2b, lower graph and error bars).

The uncertainty on the O₂ effective cross section varies roughly from 1 to 30% depending on the spectral region and the pressure. At the maximum intensity of nonsaturated lines, the error is about 1–5%; 5–15% are usual values between lines, and in the region above the dissociation limit, the error reaches 10–15%. Similarly, the errors in $\sigma_{O_2-O_2}$ and σ_{O_2HC} are of the same order of magnitude. Toward the visible part of the spectrum where absorbances or cross sections are close to zero, high percentage errors are obtained. To evaluate better the accuracy in the latter case, absolute errors are given. In Fig. 2a and 2b, the cross-sections $\sigma_{O_2-O_2}$ and σ_{O_2HC} are presented together with their errors (lower parts and error bars on the main plot). The error increases with the intensity of the lines, which become saturated at high pressure, but also for wavenumbers larger than $40\,000 \text{ cm}^{-1}$, due to the cutoff of the lamp's emissivity.

3.3. The Wulf Bands

Figure 1a shows the total absorbance resulting from the Herzberg bands and their underlying continuum overlapped by the diffuse triplet Wulf bands. Figure 2a (and also Fig. 5) presents the absorption cross section corresponding to the Wulf bands calculated by the procedure described in Section 3.1.

The pressure effect on the Wulf bands can be evaluated from

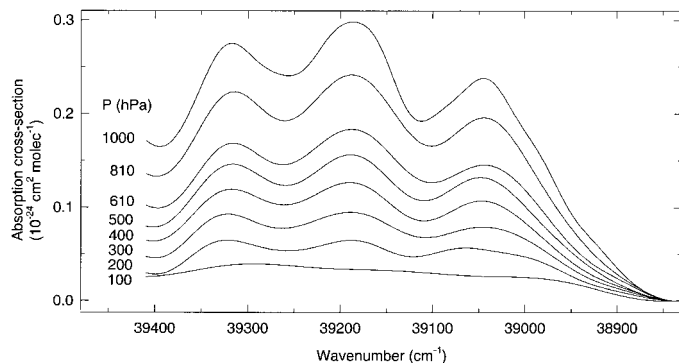


FIG. 3. Pressure effect on the structure and position of the 7–0 Wulf band. The cross sections are vertically shifted to zero at 38 840 cm^{-1} for a better comparison.

Fig. 3 (see also Fig. 1c). From the pressure range of this study, it appears clearly that the shape and position of the triplets are independent of the gas pressure. Only their strength increases with pressure, as already pointed out by Dianov-Klokov (11).

3.3.1. Vibrational analysis. The positions of the triplets are presented in Table 2 and compared with literature data. We failed to detect the 0–0 and 1–0 bands. The 11–0 and 12–0 triplet positions are difficult to determine because of the overlapping of the triplet structures when v' increases, as is shown in Fig. 2a and Fig. 5. Considering the broadness of the peaks, the absolute positions are in good agreement with the results of previous authors. The constant decrease of the distance between the bands is characteristic of a converging band progression. This is illustrated in Fig. 4a, where the $\Delta G(v)$ values corresponding to the energy separation between successive bands are presented: $\Delta G(v)$ varies from ~ 800 to $\sim 300 \text{ cm}^{-1}$ for $v' = 1$ to 10. Our data are the most uniform, but the so far unexplained anomaly detected by others at $v' = 8$ (8–10) is still observable as a slight break in the straight line. Because band origins cannot be determined for the diffuse triplets, the $\Delta G(v)$ plotted in Fig. 4 are the differences between wavenumbers measured at the maxima of the bands.

In Fig. 4b, the $\Delta G(v)$ values of the Wulf bands and of the $A' \ ^3\Delta_u$ state are compared. The latter are obtained from our recent rotational analysis of the $A' \ ^3\Delta_u$ state (24). The intervals between the peaks are consistent with previous studies (9, 10). They are close to the values of the triplet splittings for the $A' \ ^3\Delta_u$ state, which vary from 149.6 to 118.2 cm^{-1} for $v' = 2$ to 11, according to the spin–orbit coupling constants A derived by Jenouvrier *et al.* (24).

Strong similarities between the diffuse triplets and the $A' \ ^3\Delta_u \leftarrow X^3\Sigma_g^-$ transition, in terms of relative positions and triplet splitting, are thus demonstrated. These results reinforce the conclusions of previous studies (6, 20–22) that the Wulf bands are due to an enhancement of the forbidden $A' \ ^3\Delta_u \leftarrow X^3\Sigma_g^-$ transition caused by the relaxation of the dipole-forbidden selection rule during collision.

3.3.2. Absorption cross section in pure oxygen. The collision-induced absorption cross-section $\sigma_{\text{O}_2\text{-O}_2}$ at room temperature is presented in Fig. 5, together with a comparison to literature data.

To our knowledge, there are only two papers presenting a complete Wulf bands absorption cross section (from $\sim 34\,000 \text{ cm}^{-1}$ to the dissociation limit) in pure oxygen at room temperature (12, 17). Zelikina *et al.* (17) studied compressed and liquid oxygen, taking advantage of the fact that at these very high pressures the absorption of the Herzberg bands becomes negligible. Only Shardanand (12) made measurements at various pressures and separated the O_2 and the $\text{O}_2\text{-O}_2$ contributions by a least-squares linear regression. Several other papers (14, 19, 33–35) deal with the region above the dissociation

TABLE 2
Wulf Bands Positions and Comparison
with Literature Data

Wulf (8)	Finkelburg & Steiner (9)	Herman (10)	This work
$v \text{ (cm}^{-1}\text{)}^\#$	$v_{\text{vac}} \text{ (cm}^{-1}\text{)}^\ddagger$	$v_{\text{vac}} \text{ (cm}^{-1}\text{)}^\ddagger$	$v_{\text{vac}} \text{ (cm}^{-1}\text{)}^\ddagger$
0-0		34190	
		34319	
		34425	
1-0		35016	
35002	35139	35176	
		35300	
2-0	35755	35768	35773
35804	35909	35910	35923
	36025	36022	36063
3-0	36486	36488	36509
36556	36619	36621	36657
	36740	36744	36790
4-0	37164	37166	37210
37244	37330	37312	37353
	37411	37420	37467
5-0	37839	37829	37861
37879	37982	37973	38003
	38084	38068	38134
6-0	38450	38408	38473
38499	38584	38594	38617
	38703	38712	38746
7-0	39036	39052	39044
39085	39158	39150	39186
	39312	39305	39317
8-0	39592	39596	39576
39714	39702	39718	39712
	39829	39821	39830
9-0	40036	40030	40029
40161	40165	40169	40167
	40294	40278	40289
10-0	40424	40433	40420
	40556	40554	40551
	40671	40696	(40686)*
11-0	40971		(40686)*
			40870
			40975

$\# v$ = Mean position of the bands; $\ddagger v_{\text{vac}}$ = Vacuum wavenumber;

* = Triplets are superposed due to converging bands.

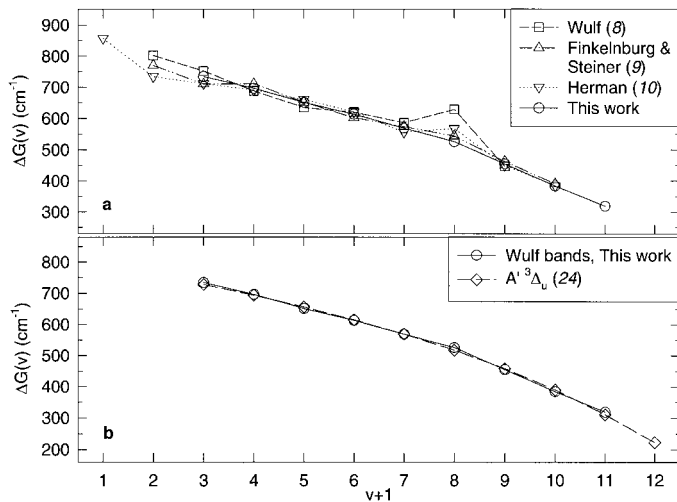


FIG. 4. Relative positions of the Wulf bands: Wavenumber interval between the central peaks of each triplet and comparison (a) with literature data, (b) with the $A' \ ^3\Delta_u$ state.

limit and gave data for wavenumbers greater than $40\,000\text{ cm}^{-1}$. These literature data, described as “the pressure-dependent component of the Herzberg continuum,” are shown in Fig. 5. One can clearly see that the most recent experimental values given by Yoshino *et al.* (35) connect well with the Wulf bands, which suggests that their values can be attributed to the Wulf continuum.

The collision-induced absorption cross-section $\sigma_{\text{O}_2\text{-O}_2}$ is in good agreement with earlier results, despite the different pressure ranges used in the studies. Our higher resolution results

improve the accuracy of the absorption cross section in the region of the Wulf bands.

3.3.3. Absorption cross sections in gas mixtures. In this work, spectra were recorded at constant X/O_2 mixing ratio (with $X = \text{N}_2$ or Ar) with increasing total pressure.

Figure 6 compares the σ' cross sections of pure O₂ and of O₂- X mixtures (with $X = \text{N}_2$ or Ar) at the same total pressure. From these experiments, several conclusions can be drawn.

First, they show that the intensity of the Wulf bands depends on the *total* pressure, and that the shape and position of the triplets are independent of the nature of the gas in the pressure range and spectral interval of this study. In other words, the Wulf bands exhibit the same features whatever the collisional partner. This observation provides additional evidence to that presented earlier (23) that the Wulf bands are produced by collision-induced absorption (CIA) and not from dimer absorption.

Second, it can be seen in Fig. 6 that the differences (a)–(b) and (a)–(c) between O₂-O₂ and O₂- X cross sections recorded at the same total pressure are nonzero and increase slightly on the UV side, but show no obvious triplet structure. To our knowledge, the fact that the differences do not contain any triplet structure, implying that the intensities of the O₂-O₂ and O₂- X triplets are in the ratio of 1:1, was never mentioned before. If the reliability of the differences is not obvious since they are of the same order of magnitude ($0.5 \times 10^{-24}\text{ cm}^2\text{ molecule}^{-1}\text{ atm}^{-1}$) as the experimental error, the good agreement between our collision-induced cross sections and the literature data (Figs. 5 and 7, see below) allow us nevertheless to assume that they are real. In addition, the differences are

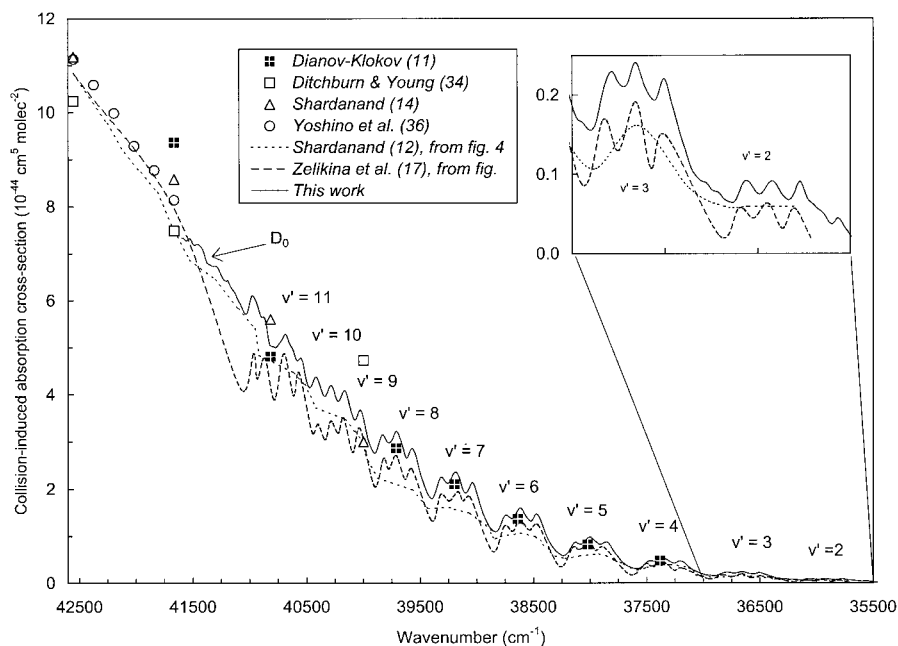


FIG. 5. The O₂-O₂ collision-induced absorption cross section and comparison with literature data.

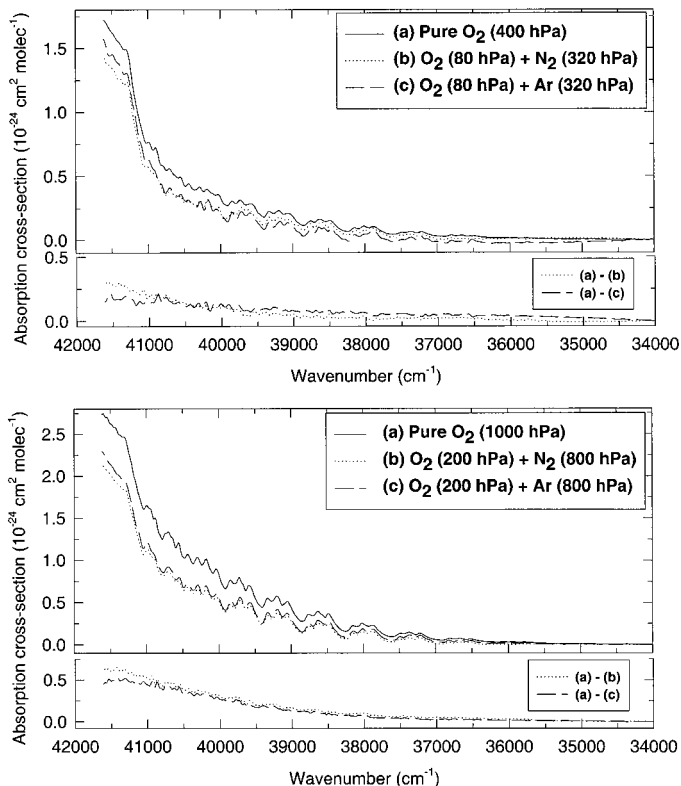


FIG. 6. Comparison of absorption cross sections (corresponding to σ' given in Eq. [3]) of oxygen in pure O_2 and in mixtures with N_2 or Ar . The bottom part of each figure represents the differences between the two spectra of the upper part.

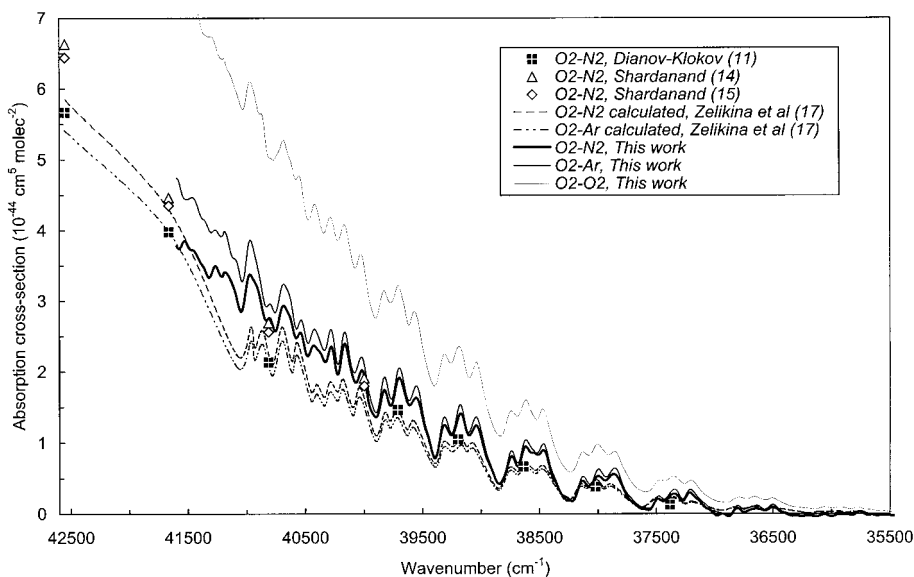


FIG. 7. Comparison of the O_2 - X collision-induced absorption cross sections (bold solid line for O_2 - N_2 and normal solid line for O_2 - Ar) with literature data (dashed lines and markers). The O_2 - O_2 collision-induced absorption cross section (thin solid line) is also drawn for comparison. The data of Zelikina *et al.* (17) are calculated from their O_2 - O_2 absorption coefficients (μ_{11}) and their mean ratios $\sigma_{O_2-N_2}/\sigma_{O_2-O_2}$ and $\sigma_{O_2-Ar}/\sigma_{O_2-O_2}$ (γ_{12}); the latter is calculated by the authors to be the same in the triplet region as in the 200–240 nm region.

directly proportional to the total pressure; they are most probably due to a collision-induced continuum arising only from O_2 - O_2 interactions.

Third, O_2 - N_2 and O_2 - Ar cross sections are practically equal, which means that N_2 and Ar act with nearly the same efficiency to induce absorption in the pressure range used in this study.

The O_2 - N_2 and O_2 - Ar collision-induced absorption (CIA) cross sections, calculated as explained in Section 3.1, are presented in Fig. 7. The O_2 - O_2 CIA cross section is also drawn in this figure for comparison. The almost equal O_2 - N_2 and O_2 - Ar CIA cross sections agree well with previous studies (11, 14, 15, 17), despite the high degree of uncertainty (up to 100%) generated by a limited data set, numerous steps in the procedure, and extreme experimental conditions. One should also point out that σ_{O_2-X} is obtained from Eq. [3] by subtracting the $\sigma_{O_2-O_2}$ contribution; this implies that, in the O_2 - X mixture, the collision probability between O_2 and X molecules and the collision probability between O_2 molecules are assumed identical. This is a reasonable assumption as O_2 and N_2 molecules are both homonuclear with comparable diameter and mass and thus show similar polarizabilities.

Values for the ratio $\sigma_{O_2-O_2}/\sigma_{O_2-N_2}$ can be obtained from the literature (11, 14, 15, 17, 19). These ratios range between 1.6 and 2.5 in the Wulf bands region and are most often close to 2.0, as shown in Table 3. We obtain a mean ratio of 1.8 ± 0.1 measured at the positions of the central triplet peak. The ratios at the 2–0 and 3–0 band positions are not calculated because CIA cross sections are close to zero.

TABLE 3
O₂-O₂ and O₂-X Collision-Induced Absorption Cross-Section Ratios $\sigma_{O_2-O_2}/\sigma_{O_2-X}$, and Comparison with Literature Data

	ν (cm ⁻¹)	DK N2	S1 N2	S2 N2	Z N2	Z Ar	O N2	This work N2	This work Ar
2-0	35923							#	#
3-0	36657							#	#
4-0	37353							1.90	1.58
5-0	38003	2.26						1.85	1.58
6-0	38617	2.07						1.69	1.54
7-0	39186	2.00						1.69	1.55
8-0	39712	1.94						1.72	1.61
	40000		1.63	1.70				1.79	1.66
9-0	40167							1.71	1.60
	40323						2.52	1.87	1.72
10-0	40551							1.80	1.63
	40816		2.13	1.92				1.83	1.71
11-0	40870	2.28						1.81	1.59
	41098							1.93	1.67
	41406							1.96	1.65
	41667	2.35	1.92	1.80	1.78	2.27		1.97	1.55
	42553	(2.21)	1.69	1.72					
	43478		1.95	1.78	1.48	1.77	2.17		
	44444		1.96	1.79					
	45455		2.07	1.94	1.83	1.87			
	46511		2.13	2.06					
	47619		2.29	2.24	2.02	1.94			
	48781		2.51	2.46					
	50000		3.06						
		1.85±0.21 [†]		2.00±0.16 [‡]		1.8±0.1*		1.7±0.1*	

DK = Data of Dianov-Klokov (Table 2 in ref. 11); S1 = calculated from $\sigma_{O_2-O_2}$ and $\sigma_{O_2-N_2}$ of Shardanand (14); S2 = calculated from $\sigma_{O_2-O_2}$ and $\sigma_{O_2-N_2}$ of Shardanand (15); Z = calculated from $\sigma_{O_2-O_2}$ and $\sigma_{O_2-N_2}$ of Zelikina *et al.* (17); O = calculated from $\sigma_{O_2-O_2}$ and $\sigma_{O_2-N_2}$ of Oshima *et al.* (19); N2 = $\sigma_{O_2-O_2}/\sigma_{O_2-N_2}$, Ar = $\sigma_{O_2-O_2}/\sigma_{O_2-Ar}$; # = CIA cross-sections close to 0; † = Data of Zelikina *et al.* (Table 4 in ref. 17); * = Average and standard deviation of the given values.

The dependence of the ratio $\sigma_{O_2-O_2}/\sigma_{O_2-N_2}$ with wavelength has been considered in the literature: Horowitz *et al.* (22) deduced a constant ratio in the 205–240 nm region (48 780–41 670 cm⁻¹); Zelikina *et al.* (17) commented that the ratio is the same in the triplet region as in the 200–240 nm region; and Shardanand (14) obtained an increasing trend of the ratio with wavenumber in the 200–250 nm region. Our results show a relatively constant ratio at the positions of the central triplet peak and also in the 41 000–42 000 cm⁻¹ wavenumber region (see Table 3), but this constant ratio does not hold for wavelengths situated between the peaks, in agreement with the lack of structures in the differences presented in Fig. 6.

Straightforward conclusions concerning the difference between O₂-O₂ and O₂-X collision-induced absorption cannot be formulated from our results, but a general agreement is found in the literature, i.e., O₂-N₂ and O₂-Ar collisions present almost identical cross sections, lower than that of O₂-O₂ collisions by approximately a factor of 2. However, we find astonishingly that the difference presents no structure and might indicate that an additional unknown mechanism is responsible for part of the total CIA cross section.

3.4. Modeling of the Wulf Bands

The O₂-O₂ Wulf bands have been modeled using the theory of collision-induced absorption. Collision-induced transitions,

characterized by Raman-like selection rules ($\Delta J = 0, \pm 2$) have been analyzed in detail by Placzek (36), who presents Hönl-London factors for linear molecules in their ground state.

A stick spectrum was first generated, using appropriate models and constants for the two electronic levels involved. For the ground electronic state ($^3\Sigma_g^-$), the matrix elements of the Hamiltonian described by Cheung *et al.* (37) and the constants of Amiot and Vergès (38) were used. For the excited state ($A' ^3\Delta_u$), the matrix elements of Hocking *et al.* (39) were used with the revised constants of Jenouvrier *et al.* (24). The relative intensities of the different vibrational bands were deduced from the experimental integrated cross sections, which have been determined from the Herzberg III system analysis (25).

A simulated spectrum of the Wulf bands is then obtained by broadening each line with a Lorentzian line profile adjusted to best reproduce the CIA observed profiles. This profile is made asymmetric, by adding to the profile a Boltzmann factor $e^{-hc\Delta\nu/kT}$, which reflects the fact that absorption on the high-frequency side of the line is associated with an increased translational energy with respect to the low-frequency side. Bosomworth and Gush (40) have shown that a lineshape function including an exponential tail gives a better representation of the H₂ infrared lines. We have thus considered the following line profiles, already defined by Tabisz *et al.* (20),

$$\begin{aligned}
 I^+(\nu) &= \frac{I_0}{1 + (\Delta\nu/\delta)^2} & \text{for } \nu_0 < \nu < \nu_0 + 1.75\delta \\
 I^+(\nu) &= A e^{(-B\Delta\nu)} & \text{for } \nu > \nu_0 + 1.75\delta \\
 I^-(\nu) &= I^+(\nu) e^{(-hc\Delta\nu/kT)} & \text{for } \nu < \nu_0,
 \end{aligned}
 \tag{6}$$

where ν_0 is the central position of a line of intensity I_0 , δ is the half-width at half-maximum ($=70.0$ cm⁻¹ in our simulation), A and B are constants chosen so that I and its first derivative are continuous at $\nu_0 + 1.75\delta$.

Results of the model, multiplied by a constant in order to match the data, are compared to the experimental values in Fig. 8. The diffuse triplet structures, arising from the triplet nature of the upper state, are well reproduced for all the vibrational transitions taken into account. The relative intensities of the vibrational transitions are in good agreement with the experimental data. The model fails, however, to reproduce the high-wavenumber part of the spectrum, as no transitions to the continuum have been taken into account.

3.5. The Herzberg Continuum Absorption Cross Section

The Herzberg continuum, presented in Fig. 2b with error bars, is compared in Fig. 9 to a calculated curve and to literature data. The small peaks and the negative values appearing in the experimental cross section can be neglected because they are due to calculation artifacts and are not significant. The region of the Herzberg continuum below the

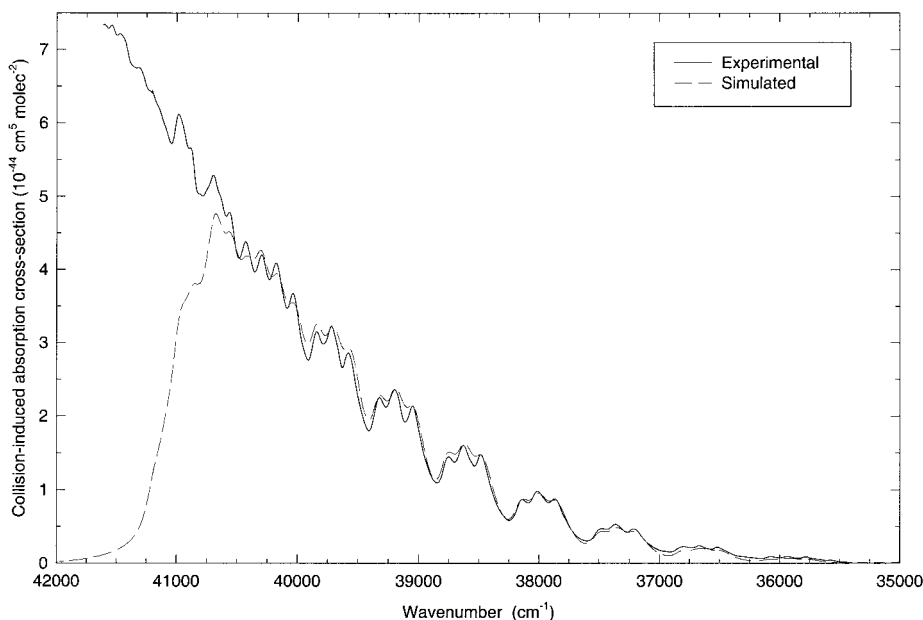


FIG. 8. Comparison between the Wulf bands obtained experimentally (solid line) and calculated by a model (dashed line) (see text).

dissociation limit represents the long wavelength extension of the bound-free Herzberg continuum into the bound region. This is illustrated in the high wavenumber part of Fig. 9 where it is seen that our experimental curve is perfectly in alignment with the literature data.

The shape of a continuum below the dissociation limit corresponds to a decreasing exponential function related to the population of the excited rotational levels in the ground state. This part of the Herzberg continuum has therefore been sim-

ulated by a cumulative Boltzmann population distribution of the rotational levels of the ground state (38), without taking into account the J dependence of the dipole transition moment. The relative intensities are multiplied by a constant to connect with the experimental data at the dissociation limit. This calculated curve is presented in Fig. 9 and agrees well with the experimental curve. One has to mention a similar study concerning the continuum which underlies the Schumann–Runge bands of O_2 : Lewis *et al.* (41) presented extensive measure-

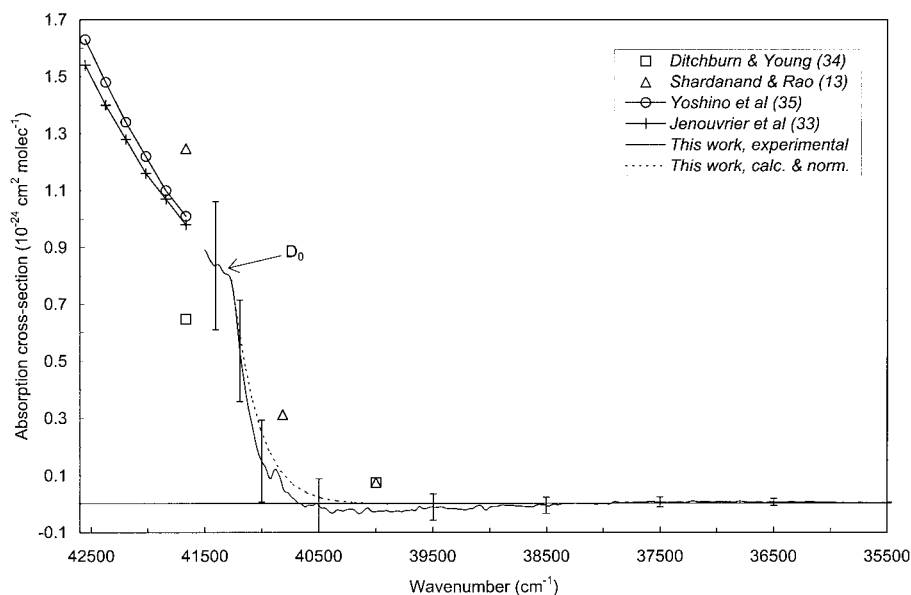


FIG. 9. Comparison of the Herzberg continuum absorption cross section obtained in this work with literature data, and with a calculated curve.

ments and theoretical calculations of the Schumann–Runge continuum absorption cross section in the 175–180 nm region and verified that the continuum is due to absorption from rotationally excited levels of the ground state.

4. ATMOSPHERIC INTEREST

These new laboratory cross-section data, combined with the O₂ line parameters obtained from fully-resolved high-resolution spectra presented previously (24), allow us to calculate a synthetic spectrum at any desired resolution and pressure. These measurements should be very useful to interpret correctly the atmospheric spectra in which the signatures of several species (aromatic hydrocarbons, ozone, etc.) strongly overlap with the oxygen spectrum. They should lead to improved concentration measurements in atmospheric studies using differential optical absorption spectroscopy (DOAS) or differential absorption light direction and ranging (DIAL), as pointed out by Volkamer *et al.* (3).

It is worth mentioning that the construction of a synthetic spectrum should be done with great care, on account of errors that the convolution technique can introduce (2, 3, 42). The usual procedure, which compares absorbances of atmospheric spectra with convoluted cross sections, produces nonlinearities of absorbance with concentration. This is because the convolution and the logarithmic functions do not commute; the cross section has therefore to be converted into a spectrum before being convoluted by an instrumental function. Moreover, the spectral absorption features in the cross section have to be fully resolved in order to avoid a dependence of lineshape with concentration.

The combined pressure effect of N₂ and O₂ depends on wavelength and its contribution to the absorbance of O₂ in the atmosphere can only be roughly assessed. In the region 41 270–42 000 cm⁻¹, the pressure effect contributes to 50–55% of the total absorbance at ground level (1000 hPa). This fraction, which decreases with increasing altitude, is still 20–25% at the tropopause (~10 km or 265 hPa) and becomes negligible (<1%) at an elevation of 35 km (5.7 hPa). Similar results have been presented by Horowitz *et al.* (Table 5 in Ref. 22) for the region 205–240 nm (48 780–41 670 cm⁻¹). In the Herzberg bands region (34 000–41 270 cm⁻¹), the contribution of the combined pressure effect is much more variable, due to the presence of the Herzberg lines. At the ground level, the pressure effect contributes to 100% of the absorbance on the baseline between the lines, and from 10 to 25% at the maximum intensity of the most intense lines of each band. This fraction also decreases with pressure.

In view of these percentages and of the recent findings of Zipf and Prasad (43) concerning the implication of the O₂–N₂ photochemistry in the production of NO_x, it appears that the absorption of solar radiation by the O₂–N₂ bands may represent an efficient source of NO/NO₂ in the stratosphere and possibly

in the troposphere. This new stratospheric NO_x source will in turn influence the ozone formation.

5. CONCLUSIONS

As part of an extensive study concerning molecular oxygen (23–26), the oxygen spectrum is examined in the UV region at low resolution (2 cm⁻¹). The study of its pressure dependence has led to the separation of the different components, i.e., the O₂ Herzberg bands, the Herzberg continuum, and the Wulf bands. New O₂–O₂ collision-induced absorption cross sections, obtained with better precision and accuracy than earlier results, are presented. The Herzberg continuum has been extended to the bound region, far below the dissociation limit.

These new laboratory data, combined with our line parameters of the Herzberg systems (24, 25), allow to calculate oxygen cross sections for any pressure condition; this in turn should improve atmospheric measurements.

In the pressure range and spectral region of this study, the intensity of the Wulf bands shows a quadratic dependence on pressure ($P_{O_2}P_X$), but their shape and position do not vary with pressure. Besides large uncertainties, it is shown that the collision-induced absorption (CIA) cross sections obtained for different O₂–*X* interacting pairs depend on the nature of the molecule *X*. The O₂–N₂ and O₂–Ar collision-induced absorption cross sections are almost equal but are about twice lower than the O₂–O₂ CIA cross section. However, the shape of the triplets bands is not modified at all.

The crude simulations performed for the Wulf bands and for the Herzberg continuum are in good agreement with the experimental results. The data are available in digital form upon e-mail request or by download from the IASB-BIRA web site (<http://www.oma.be/BIRA-IASB/Scientific/Topics/Lower/LaboBase/Laboratory.html>).

ACKNOWLEDGMENTS

This research project was funded by the Belgian State, Federal Office for Scientific, Technical, and Cultural Affairs and the Fonds National de la Recherche Scientifique (Belgium). We are grateful for support provided by the Centre National de la Recherche Scientifique and Institut National des Sciences de l'Univers (France) through the Programme National de Chimie Atmosphérique. The technical assistance provided by A. Rizopoulos and J.-P. Lux is gratefully acknowledged. We thank Dr. D. Hurtmans for kindly providing the successive versions of Winprof and many helpful suggestions to achieve the best possible simulation of the discrete part of the O₂ spectrum.

REFERENCES

1. C. Camy-Peyret, B. Bergqvist, B. Galle, M. Carleer, C. Clerbaux, R. Colin, C. Fayt, F. Goutail, M. Nunes-Pinharanda, J. P. Pommereau, M. Hausmann, U. Platt, I. Pundt, T. Rudolph, C. Hermans, P. C. Simon, A. C. Vandaele, J. M. Plane, N. Smith, *J. Atmos. Chem.* **23**, 51–80 (1996).
2. A. C. Vandaele and M. Carleer, *Appl. Opt.* **38**, 2630–2639 (1999).
3. R. Volkamer, T. Etzkorn, A. Geyer, and U. Platt, *Atmos. Environ.* **32**, 3731–3747 (1998).
4. G. Herzberg, *Can. J. Phys.* **30**, 180–210 (1952).

5. G. Herzberg, *Can. J. Phys.* **31**, 657–669 (1953).
6. A. J. Blake and D. G. McCoy, *J. Quant. Spectrosc. Radiat. Transfer* **38**, 113–120 (1987).
7. P. H. Krupenie, *J. Phys. Chem. Ref. Data* **1**, 423–534 (1972).
8. O. R. Wulf, *Proc. Natl. Acad. Sci.* **14**, 609–613 (1928).
9. W. Finkelburg and W. Steiner, *Z. Phys.* **72**, 69–88 (1932).
10. L. Herman, *Ann. Phys.* **11**, 548–611 (1939).
11. V. I. Dianov-Klokov, *Opt. Spektrosk.* **2**, 233–236 (1966).
12. R. Shardanand, *Phys. Rev.* **186**, 5–9 (1969).
13. R. Shardanand and A. D. Prasad Rao, *J. Quant. Spectrosc. Radiat. Transfer* **17**, 433–439 (1977).
14. R. Shardanand, *J. Quant. Spectrosc. Radiat. Transfer* **18**, 525–530 (1977).
15. R. Shardanand, *J. Quant. Spectrosc. Radiat. Transfer* **20**, 265–270 (1978).
16. B. Coquart and D. A. Ramsay, *Can. J. Phys.* **64**, 726–732 (1986).
17. G. Ya. Zelikina, V. V. Bertsev, and M. B. Kiseleva, *Opt. Spektrosk.* **77**, 579–583 (1994).
18. G. Ya. Zelikina, V. V. Bertsev, A. P. Burtsev, and M. B. Kiseleva, *Opt. Spektrosk.* **81**, 685–689 (1996).
19. Y. Oshima, Y. Okamoto, and S. Koda, *J. Phys. Chem.* **99**, 11830–11833 (1995).
20. G. C. Tabisz, E. J. Allin, and H. L. Welsh, *Can. J. Phys.* **47**, 2859–2871 (1969).
21. J. Goodman and L. E. Brus, *J. Chem. Phys.* **67**, 1482–1490 (1977).
22. A. Horowitz, W. Schneider, and G. K. Moortgat, *J. Phys. Chem.* **94**, 2904–2907 (1990).
23. P. Bernath, M. Carleer, S. Fally, A. Jenouvrier, A. C. Vandaele, C. Hermans, M.-F. Méridienne, and R. Colin, *Chem. Phys. Lett.* **297**, 293–299 (1998).
24. A. Jenouvrier, M.-F. Méridienne, B. Coquart, M. Carleer, S. Fally, A. C. Vandaele, C. Hermans, and R. Colin, *J. Mol. Spectrosc.* **198**, 136–162 (1999).
25. M.-F. Méridienne, A. Jenouvrier, B. Coquart, A. C. Vandaele, C. Hermans, M. Carleer, S. Fally, and R. Colin, *J. Mol. Spectrosc.* **202**, 171–193 (2000).
26. C. Hermans, A. C. Vandaele, B. Coquart, A. Jenouvrier, M.-F. Méridienne, S. Fally, M. Carleer, and R. Colin, unpublished manuscript.
27. J. P. Lux and A. Jenouvrier, *Rev. Phys. Appl.* **20**, 869–875 (1985).
28. D. R. Bates, *Planet. Space Sci.* **32**, 785–790 (1984).
29. D. Hurtmans, private communication, 1999.
30. M. Carleer, S. Fally, R. Colin, B. Coquart, A. Jenouvrier, M.-F. Méridienne, C. Hermans, A.-C. Vandaele, and P. C. Simon, ASA (Atmospheric Spectroscopy Applications) Reims '96 Workshop, 4–6/09/1996, pp. 87–90, 1996.
31. C. Hermans, A.-C. Vandaele, M. Van Roozendaal, P. C. Simon, M. Carleer, S. Fally, R. Colin, B. Coquart, A. Jenouvrier, M.-F. Méridienne, ASA (Atmospheric Spectroscopy Applications) Reims '96 workshop, 4–6/09/1996, pp. 83–86, 1996.
32. W. H. Press, S. A. Teukolsky, W. T. Vetterling, B. P. Flannery, in “Numerical Recipes in C: The Art of Scientific Computing,” 2nd ed., Cambridge Univ. Press, Cambridge, UK, (<http://www.nr.com>), 1993.
33. A. Jenouvrier, B. Coquart, and M.-F. Méridienne, *J. Quant. Spectrosc. Radiat. Transfer* **36**, 349–354 (1986).
34. R. W. Ditchburn and P. A. Young, *J. Atmos. Terr. Phys.* **24**, 127–139 (1962).
35. K. Yoshino, A. S.-C. Cheung, J. R. Esmond, W. H. Parkinson, D. E. Freeman, S. L. Guberman, A. Jenouvrier, B. Coquart, and M.-F. Méridienne, *Planet. Space Sci.* **36**, 1469–1475 (1988).
36. G. Placzek, “The Rayleigh and Raman Scattering, Handbuch der Radiologie,” (E. Marx, Ed.), Vol. 2, pp. 209–374, Akad. Verlagsgesellschaft VI, Frankfurt-am-main, 1934.
37. A. S.-C. Cheung, K. Yoshino, W. H. Parkinson, S. L. Guberman, and D. E. Freeman, *Planet. Space Sci.* **34**, 1007–1021 (1986).
38. C. Amiot and J. Vergès, *Can. J. Phys.* **59**, 1391–1398 (1981).
39. W. H. Hocking, M. C. L. Gerry, and A. J. Merer, *Can. J. Phys.* **57**, 54–61 (1979).
40. D. Bosomworth and H. Gush, *Can. J. Phys.* **43**, 751–769 (1965).
41. B. R. Lewis, L. Berzins, J. H. Carver, and S. T. Gibson, *J. Quant. Spectrosc. Radiat. Transfer* **33**, 627–643 (1985).
42. C. Hermans, A. C. Vandaele, M. Carleer, S. Fally, R. Colin, P. Bernath, A. Jenouvrier, B. Coquart, and M.-F. Méridienne, *Environ. Sci. Pollut. Res.* **6**, 151–158 (1999).
43. E. C. Zipf and S. S. Prasad, *Science* **279**, 211–213 (1998).